Géographie physique et Quaternaire, 2004, vol. 58, nos 2-3, p. X-X, X fig., X tabl.

STABLE ISOTOPE RECORDS FROM MOUNT LOGAN, ECLIPSE ICE CORES AND NEARBY JELLYBEAN LAKE. WATER CYCLE OF THE NORTH PACIFIC OVER 2000 YEARS AND OVER FIVE VERTICAL KILOMETRES: SUDDEN SHIFTS AND TROPICAL CONNECTIONS

D.A. FISHER*, C. WAKE, K. KREUTZ, K. YALCIN, E. STEIG, P. MAYEWSKI, L. ANDERSON, J. ZHENG, S. RUPPER, C. ZDANOWICZ, M. DEMUTH, M. WASZKIEWICZ, D. DAHL-JENSEN, K. GOTO-AZUMA, J.B. BOURGEOIS, R.M. KOERNER, J. SEKERKA, E. OSTERBERG, M.B. ABBOTT, B.P. FINNEY and S.J. BURNS; first, eighth, tenth, eleventh, fifteenth, sixteenth and seventeenth authors : Geological Survey of Canada, 601 Booth Street, Ottawa, Ontario K1A 0E8; second and fourth authors : Climate Change Research Center, Morse Hall, University of New Hampshire, Durham, New Hampshire 03824, United States; third, sixth and eighteenth authors : Climate Change Institute and Department of Earth Sciences, University of Maine, Orono, Maine 04469, United States; fifth and ninth authors : Quaternary Research Center, 19 Johnson Hall, Box 1360, University of Washington, Seattle, Washington 98195, United States; seventh and twenty-first authors : Department of Geosciences, University of Massachusetts-Amherst, Amherst, Massachusetts 01003, United States; twelfth author : 9553 77th Avenue, Edmonton, Alberta T6C 0M3; thirteenth author : Niels Bohr Institute, Juliane Maries Vej 30, University of Copenhagen, DK-2100, Copenhagen East, Danemark; fourteenth author : National Institute of Polar Research, Tokyo 173-8515, Japan; nineteenth author : Department of Geology and Planetary Science, University of Pittsburg; Pittsburg, Pennsylvania 15260; United States; twentieth author : Institute of Marine Sciences, University of Alaska Fairbanks, Fairbanks, Alaska 99775, United States.

ABSTRACT Three ice cores recovered on or near Mount Logan, together with a nearby lake record (Jellybean Lake), cover variously 500 to 30 000 years. This suite of records offers a unique view of the lapse rate in stable isotopes from the lower to upper troposphere. The region is climatologically important, being beside the Cordilleran pinning-point of the Rossby Wave system and the Aleutian Low. Comparison of stable isotope series over the last 2000 years and model simulations suggest sudden and persistent shifts between modern (mixed) and zonal flow regimes of water vapour transport to the Pacific Northwest. The last such shift was in A.D. 1840. Model simulations for modern and "pure" zonal flow suggest that these shifts are consistent regime changes between these flow types, with predominantly zonal flow prior to *ca*. A.D. 1840 and modern thereafter. The 5.4 and 0.8 km asl records show a shift at A.D. 1840 and another at A.D. 800. It is speculated that the A.D. 1840 regime shift coincided with the end of the Little Ice Age and the A.D. 800 shift with the beginning of the European Medieval Warm Period. The shifts are very abrupt, taking only a few years at most.

RÉSUMÉ *Comportement des isotopes stables dans les carottes de glace des monts Logan et Eclipse et les sédiments lacustres du lac Jellybean. Le cycle de l'eau dans le Pacifique nord sur 2000 ans et sur cinq kilomètres verticaux : changements brusques et connexions tropicales.* Trois carottes de glace prélevées à proximité du mont Logan, combinées à une coupe stratigraphique du lac Jellybean, couvrent une période comprise entre 500 et 30 000 ans. Elles renseignent sur les taux de changement de la composition isotopique de la troposphère. La région étudiée est importante au niveau climatologique puisqu'elle est au point de convergence des ondes de Rossby et de la dépression des Aléoutiennes. La comparaison entre la composition isotopique depuis 2000 ans et les résultats des simulations suggère des changements brusques et persistants entre les régimes de transport de vapeur d'eau modernes et zonaux dans le nord-est du Pacifique, où le dernier changement s'est produit en 1840 de notre ère. Les simulations indiquent que les changements de flux correspondent aux changements de régime, avec un flux zonal avant *ca* 1840 pour passer au type moderne ensuite. Les forages à 5,4 et 0,8 km d'altitude montrent un changement en A.D. 1840 et un autre en l'an 800. On présume que ces changements de régime coïncident respectivement avec la fin du Petit Âge Glaciaire et le début de la période médiévale chaude, ces changements s'étant produits en quelques années seulement.

Manuscrit reçu le 5 mai 2005 ; manuscrit révisé accepté le 13 janvier 2006 (publié le Xe trimestre 2006)
* E-mail adress: david.fisher@nrcan.gc.ca

INTRODUCTION

In Holocene times outside the tropics, stable isotopes of water given in terms of oxygen [$\delta(^{18}O)$] and deuterium [$\delta(D)$] are usually correlated geographically and temporally to the temperature of the site (Dansgaard *et al.*, 1973; Jouzel *et al.*, 1984). The standard unitless measure of ratio, d, is:

$$\delta(D) = 1000 * (([D]/[H])_{sample} - ([D]/[H])_{SMOW}) / ([D]/[H])_{SMOW}$$

where SMOW denotes "standard mean ocean water". Stable isotopic ratios are also affected by the water cycle history between the sources and the site and a generous amount of stratigraphic local noise (Fisher, 1992; Fisher *et al.*, 1996). The deuterium excess, d, is a derived variable ($d = \delta(D) - 8*\delta(^{18}O)$) that is a conserved quantity for each source region (Merlivat and Jouzel, 1979; Johnsen *et al.*, 1989). Although it is also sensitive to water cycle history that bears the moisture to the sites (Fisher, 1991; Fisher *et al.*, 1996), d is an indicator of the source ocean temperature. The geographic distribution of $\delta(^{18}O)$ and $\delta(D)$ has been modeled with the help of GCMs (Jouzel *et al.*, 1997) and intermediate complexity models (Fisher, 1990, 1992; Kavanaugh and Cuffey, 2003). The latter are used to interpret the results presented here.

Previous work on the 300-years-long Mount Logan $\delta(^{18}O)$ series (Holdsworth *et al.*, 1992; Fisher, 2002) demonstrated that it is out of phase with other proxy temperature series, showing a Little Ice Age with "warmer," more positive, values. At 5 400 m asl, $\delta(^{18}O)$ is not a temperature indicator, and a goal of this paper is to explain what it does indicate.

Three ice cores on and near Mount Logan were obtained by a Geological Survey of Canada (GSC)-led consortium of American, Japanese and Canadian groups. The stable isotopes of two of these cores and the isotopic record from Jellybean Lake just south of Whitehorse are compared. The specifics of the various core sites are given in Table I and Figure 1.

PROSPECTOR RUSSELL COL, PRCOL ICE CORE

The top of the Mount Logan massif is a 5 400 m asl plateau about 10 x 25 km dotted with several ~700-metre-high cones, the tallest of which is Mount Logan (Fig. 1B). Between the cones are relatively flat areas with low ice velocities. Figures 1C and D show the topography of the PRCol drill site and the 300-years NWCol ice core obtained in the early 1980s (Holdsworth *et al.*, 1992). The surface topography and velocities suggest that the PRCol drill site is presently close to a centre of flow. Given the low annual temperature and lack of uncovered area for ice to expand into, this situation has probably been stable over the Holocene. Older ice is within the bottom-most 5 % of the thickness and possibly affected by flow discontinuities. Here, however, we are focusing on the isotope record from only the last 2 ka, which are well away from the bed. Solid electrical conductivity records (ECM) correlate with volcanic acid horizons (Hammer, 1983). Figure 2 shows a comparison between Eclipse and PRCol records. The PRCol record is placed on a time scale using a model, recent accumulation rates and the major ECM (acid) peaks of Katmai, Laki, a large unknown peak at A.D. 1516 and White River (Clausen *et al.*, 1995; Clague *et al.*, 1995; Zheng *et al.*, 1998; Yalcin and Wake, 2003). The unidentified A.D. 1516 event must be "local" because, although it is the largest peak in the last 550 years, it has no prominence in the Eastern Arctic (Clausen *et al.*, 1995; Zheng *et al.*, 1998). Between the fixed points of this time scale, the uncertainty could be ±3 years. The White River candidate ECM peak stands out and is within a metre of where it is expected. Thus, it is assigned the age of the most recent large eruption (A.D. 803) that deposited the white ash layer over most of southern Yukon (Clague, 1995). Using the time scale for PRCol described in the text, the six largest PRCol ECM peaks coincide with six large sulfate peaks of the Eclipse core over the 530 years. Presently, ages beyond A.D. 803 are only pinned by a very clear transition into ice-age ice with a sudden reduction in ECM coinciding with a large drop in $d(^{18}O)$ (Wolfe *et al.*, 1997). This transition is assigned the Greenland date of 11 550 cal BP (Johnsen *et al.*, 1997).

By scanning 100-years segments of the Eclipse sulfate series across the PRCol ECM time series, correlation coefficients between 0.22 and 0.33 were found always with a relative lag time of ≤2 years. Allowing for these series' low autocovariance, the correlations are significant at the 95 % confidence level. The time lag was close to 0 near the three pinning points. The only century in which the correlation was not significant at 95 % was A.D. 1770-1670, when the peaks are in phase but larger in PRCol. This difference could be due to noise, or because these peaks are from more distant sites and show up more plainly at the higher site. Peaks numbered

TABLE I

Specificities of core sites

Site	Elevation (m asl)	Latitude	Longitude	Mean temperature (°C)	Main Institutions	Maximum age (BP)	Ice accumulation rate (m/yr)	Depth reached (m)
PRCol	5340	60.59	140.50	-29	GSC, UMaine	30 000	~0.65	188 (bed)
Eclipse	3017	60.51	139.47	~-5	UNH, UMaine	~1000	1.38	345
King Col	4135	60.58	140.60	-17	NIPR	~300	~1.00	220.5
Jelly Bean Lake	800 (1650)	60.35	134.80	-1	Umass, UPitt, UAF	~7500	n/a	n/a

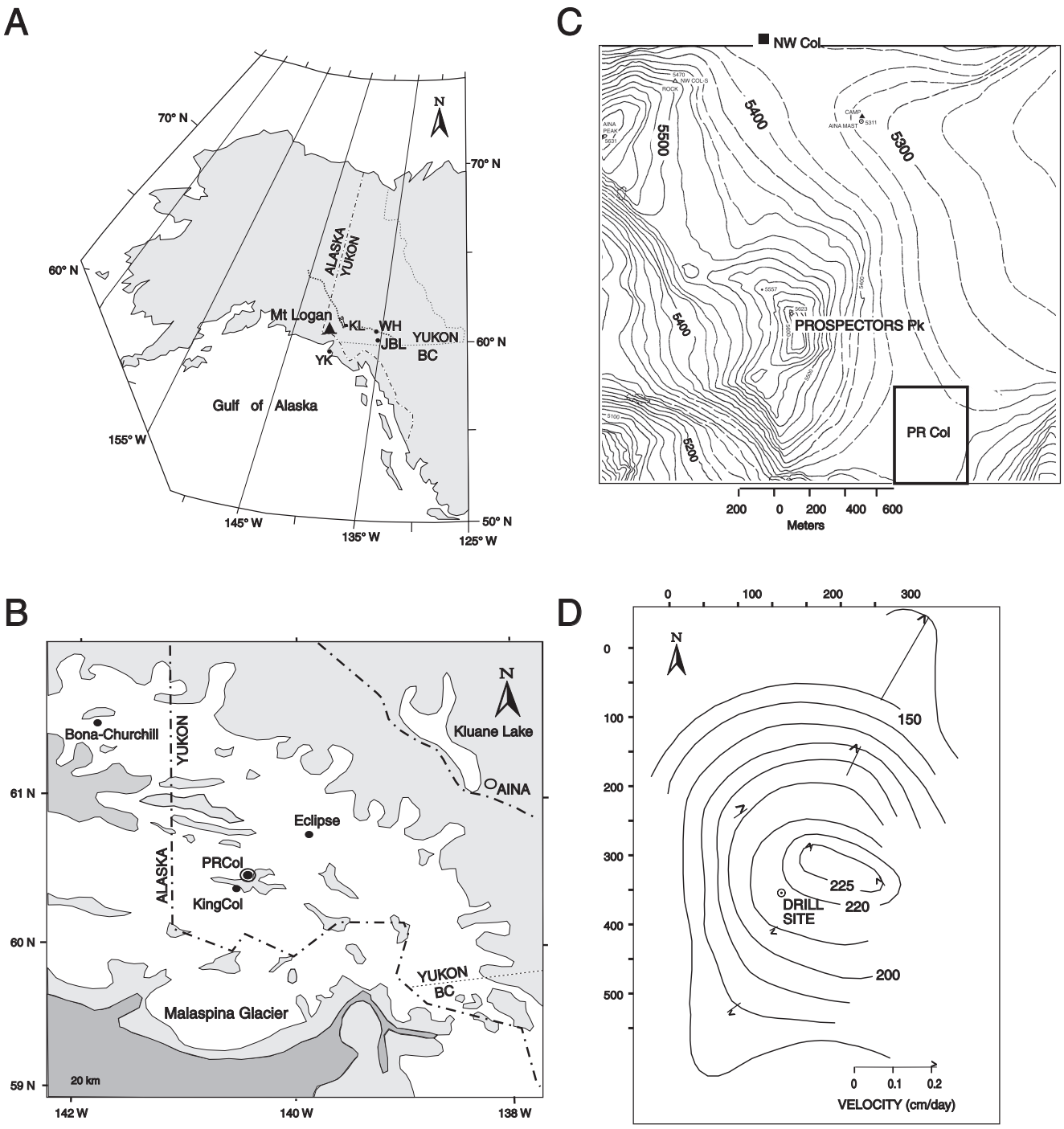

FIGURE 1. Study site locations. (A) Location of Mount Logan, Jellybean Lake (JBL), Whitehorse (WH) and Kluane Lake (KL). (B) Location of the ice core sites. (C) Surface topography for the PRCol and the older NWCol drill sites with contours in metres above sea level. The PRCol drill site is close to the centre of the rectangle at the bottom. The surface here is flat and horizontal. The PRCol weather station is close to the drill site. (D) Ice thickness (metres) and horizontal velocity map. The drill site is close to the zero-velocity point of this map.

Sites d'étude. (A) Localisation du mont Logan, du lac Jellybean (JBL), de Whitehorse (WH) et du lac Kluane (KL). (B) Localisation des sites de forage. (C) Topographie des sites PRCol et NWCol. Le site de forage de PRCOL se situe au centre du rectangle. Cette surface est plane et à l'horizontale. La station météorologique de PRCol se situe à proximité du site de forage. (D) Épaisseur de la glace (en mètres) et carte de vélocité.

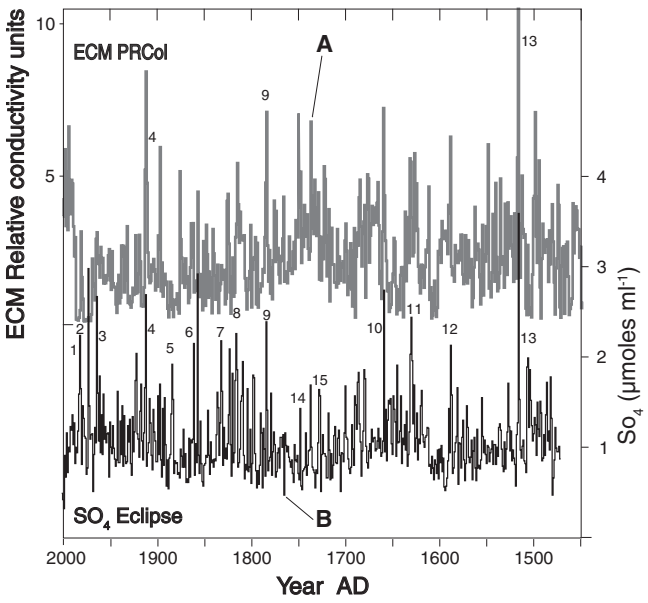

FIGURE 2. A 530-years ECM record for the PRCol core compared to the sulfate concentration from the Eclipse core. The ECM record mainly reflects the acidity of the core whose peaks are mostly volcanically derived. The sulfate is also a volcanic eruption marker, although some volcanic events give off large amounts of HCl. For example, Katmai (A.D. 1912) is a very strong chloride event in the St. Elias Mountains. The A.D. 1516 unknown event is the largest peak recorded in the Eclipse and PRCol. Peaks numbered 4, 9 and 13 (Katmai, Laki and unknown) were used to establish the PRCol time scale. Named peaks in the Eclipse core are: (1) El Chichon, (2) Tiatia, (3) Sheveluch, (4) Katmai, (5) Krakatoa, (6) Fuego, (7) Babuyan, (8) Tambora, (9) Laki, (10) Katla, (11) Furnas-Vesuvius, (12) Billy Mitchell, (13) unknown A.D. 1516.

La série temporelle de conductivité électrique du forage de PRCol est comparée à la concentration en sulfate du forage d'Eclipse sur 530 années. Cette série est le reflet de l'aciditée, où les valeurs maximales sont associées à l'activité volcanique. Le sulfate est un marqueur des éruptions volcaniques, et plusieurs événements ont produit de fortes quantités de HCl. Par exemple, l'éruption de Katmai (A.D. 1912) a produit une quantité importante de chlore sur le mont St-Elias. L'éruption inconnue de l'an 1516 constitue l'événement le plus important pour les forages d'Eclipse et de PRCol. Les maximums 4, 9 et 13 (Katmai, Laki et inconnu) sont utilisés pour établir l'échelle temporelle de PRCol. Les pics du forage d'Eclipse sont les suivants : (1) El Chichon, (2) Tiatia, (3) Sheveluch, (4) Katmai, (5) Krakatoa, (6) Fuego, (7) Babuyan, (8) Tambora, (9) Laki, (10) Katla, (11) Furnas-Vesuvius, (12) Billy Mitchell, (13) inconnu A.D. 1516.

4, 9 and 13 in the PRCol record are major sulfuric acid peaks and 4 (Katmai) is high in both sulfuric and hydrochloric acid, as it is uniquely in the Eclipse record.

ECLIPSE ICEFIELD

Two cores (345 and 130 m) were recovered in 2002 (Table I). The presence of discrete ice layers in the Eclipse ice core accounting for 5 % of the net accumulation by weight demonstrates that a limited amount of surface melting occurs at the Eclipse site during summer. Meltwater percolation does not significantly alter the glaciochemical records of the Eclipse ice core, as evidenced by the preservation of clear seasonal signals in the major ion and oxygen isotope records. This allows dating of the cores via multi-parameter annual layer counting.

Age control on the chronology established via annual layer counting is provided by the A.D. 1963 and A.D. 1961 ^{137}Cs reference horizons as well as volcanic reference horizons (Katmai, 1912; Tambora, 1815; Laki, 1783; Kuwae, 1453) developed through statistical analysis of the high-resolution sulfate record. In some cases, these identifications have been independently verified using tephrachronology.

The cores (except for the top 60 metres of the 345 m core that was drilled with a titanium barrel for trace element analyses) were sampled continuously at high resolution for major ions and stable isotopes to establish a detailed chronology. Sample resolution ranged from 6 to 15 cm for major ions and 2 to 15 cm for stable isotopes. Stringent core processing techniques were used to ensure samples were free of contamination at the ng g^{-1} level. Blanks prepared on a frequent basis showed no contamination of samples during processing of the core. Samples were analyzed for major ions (Na^+, NH_4^+, K^+, Mg^{2+}, Ca^{2+}, Cl^-, NO_3^-, SO_4^{2-}, $C_2O_4^{2-}$) via ion chromatography using a 0.5 ml sample loop in a dedicated laboratory at the University of New Hampshire Climate Change Research Center. The cation system used a CS12A column with CSRS-ultra suppressor in auto suppression recycle mode with 20 mM MSA eluent. The anion system used an AS11 column with a CSRS-ultra suppressor in auto suppression recycle mode with 6 mM NaOH eluent. Oxalate was not quantified in the 1996 core. Stable isotopes (d(^{18}O) and d(D)) were analyzed at the University of Maine Stable Isotope Laboratory with an Autoprep CO_2 equilibration system coupled to a VG SIRA instrument. A section of each core was analyzed for radionuclides (^{137}Cs) via gamma spectroscopy.

Annual layers were identified by summer-to-winter variations in the oxygen isotope ratio and sodium concentrations. The annual cycle of maxima in summer precipitation and d(^{18}O) minima in winter precipitation observed at Eclipse and other ice core sites is related, at least in part, to the temperature at which evaporation and condensation occur (Fisher, 1996). The annual cycle of sodium concentration maxima in winter and minima in summer is related to pronounced seasonal changes in the influx of marine aerosols (Whitlow *et al.*, 1992). Increased storminess and higher wind speeds in the Gulf of Alaska during winter result in enhanced entrainment of sea salt aerosols and more frequent advection of marine air masses into the St. Elias Mountains in winter, producing the winter peaks in sodium concentrations.

JELLYBEAN LAKE

Jellybean Lake (JBL) is a small (0.4 km^2), relatively deep (11.6 m) lake located 800 m asl. The lake basin is groundwater-fed from a confined aquifer recharged 12 km to the east on a broad ridge ~1 640 m asl. Inflow and outflow are sub-surface. The water column is thermally unstratified and chemically mixed. International Atomic Energy Agency precipitation data from Mayo and Whitehorse form a local meteoric water line and define the isotope values for unmodified mean annual

precipitation. The value, ~-21‰ SMOW, corresponds with local spring water and Jellybean Lake water. Although other lake data in the southern Yukon indicate a range of d(^{18}O)-variability due to evaporation of up to 10‰, water residence times in Jellybean Lake are apparently too short for evaporation to modify the lake-water d(^{18}O). The d(^{18}O) of the Jellybean Lake surface sediment calcium carbonate was -19.9‰ VPDB, and demonstrates isotopic equilibrium between calcite and water. Thus, changes in sedimentary carbonate d(^{18}O) are inferred to reflect changes in lake-water d(^{18}O) that, in turn, reflect changes in input-water d(^{18}O). The latter is controlled by regional climate (Anderson, 2004).

Sediment cores were retrieved from the deepest part of Jellybean Lake and continuously sampled at high resolution for oxygen and carbon isotopes. Lake-water calcium concentrations are sufficient to sustain bioinduced calcification such that carbonate sedimentation occurs at all water depths, and core sediments are nearly pure authigenic micrite. Samples were freeze dried, examined for purity and powdered before sub-sampling, CO_2 extraction and isotope mass spectrometry.

The Jellybean Lake calcite $\delta(^{18}O)$ is on the PDB scale, which is very close to the $\delta(^{18}O)$ of the ambient lake water on the SMOW scale (Anderson, 2004). Our method has taken the difference between calcite $\delta(^{18}O)$ shifts in PDB over certain time intervals and compared them with the differences between water in VSMOW. The conversion from VPDB to VSMOW for calcite in lake water is temperature dependent. The temperature fractionation factor is small (-0.25 ‰ per °C). Thus, if the temperature at A.D. 1840 changed by 2 °C, the per mil values could have changed by ±0.5‰. So the "temperature-error" in the A.D. 1840 Jellybean Lake shift of 1.5‰ is, at most, ±0.5‰.

The sediment core chronology is based on ^{210}Pb, ^{137}Cs, seven AMS ^{14}C measurements on identifiable macrofossils and the White River tephra (Clague *et al.*, 1995). A linear interpolation between dated depths was used to determine ages of sediment samples. The chronology indicates a fairly uniform sedimentation rate of about 0.05 to 0.075 mm a^{-1}. Based on sedimentation rates and sample thickness, the oxygen and carbon isotope samples integrate 3 to 6 years in the uppermost 16.5 cm, and 10 to 30 years for the remainder of the core that spans to about 7500 cal BP (Anderson, 2004; Anderson *et al.*, 2005).

RESULTS

SUDDEN SHIFTS IN THE MID-1800S AND A.D. 800

Figure 3A presents the last 530 years of δ(D) and $\delta(^{18}O)$ for Eclipse and PRCol cores, respectively, and Figure 3B shows the PRCol deuterium excess, d. In A.D. 1840 ±3 years, there is a 3.5 ‰ shift in $\delta(^{18}O)$ of PRCol but no shift in δ(D) of Eclipse. There is, however, a significant decrease in the Eclipse accumulation rate between A.D. 1841-1861 (Yalcin *et al.*, 2004). At the PRCol site $\delta(^{18}O)$ and d are in anti-phase (Fig. 3A-B). The A.D. 1840 shift in d ranges from pre-A.D. 1840 values of ~15 ‰ to post values of ~19 ‰. There is also a similar marked shift in $\delta(^{18}O)$ in the NWCol core (Holdsworth *et al.*, 1992), which also marks the beginning of an increase in accumulation rates (Moore *et al.*, 2002).

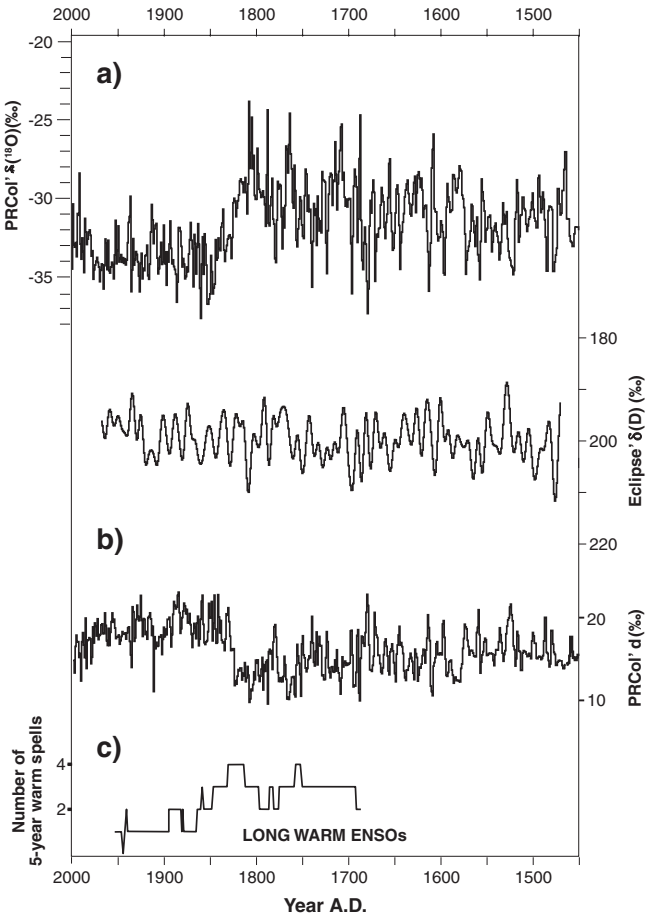

FIGURE 3. (A) The $\delta(^{18}O)$ for PRCol (5 340 m asl) and the δ(D) for Eclipse (3 017 m asl) ice core sites, smoothed with a 5-years low pass filter. At PRCol there is an abrupt shift in $\delta(^{18}O)$ of about 3 ‰ *ca.* A.D. 1840, that is not evident in the Eclipse record. The older NWCol Logan core also has a similar shift at the same date. We suggest that prior to A.D. 1840 the moisture flow was predominantly zonal with North Pacific sources of water, and after A.D. 1840 the flow was mostly "modern" delivering moisture from more southerly sources. The higher site receives relatively much more distant southern warm-source moisture than the lower. Compare the A.D. 1840 shift to that of A.D. 1976. (B) The deuterium excess plot for PRCol, indicating a major shift of moisture source *ca.* A.D. 1840. The larger excess points to warmer source oceans providing the moisture. (C) A plot of ENSO strength statistics implying that a regime shift occurred in the mid-19th century. The synoptic situation that would go along with the shift is that a deeper more northwest-centred Aleutian Low would draw moisture from farther south.

(A) Séries temporelles de $\delta(^{18}O)$ et δ(D) lissées sur 5 ans avec un filtre passe-bas pour les forages de PRCol (5 340 m asl) et d'Eclipse (3 017 m asl). On observe un changement brusque d'environ 3 ‰ de $\delta(^{18}O)$ en A.D. 1840 dans le forage de PRCol, qui ne s'observe pas dans le forage d'Eclipse. Le forage de NWCol montre un comportement similaire à celui de PRCol. On pense que le flux d'humidité est zonal en A.D. 1840, avec des sources provenant du Pacifique nord tandis qu'après A.D. 1840, il est alimenté par des sources plus au sud. Le plus haut site reçoit plus d'humidité d'une source chaude méridionale que le site le plus bas. (B) Le diagramme d'excès de deutérium du forage de PRCol suggère un changement majeur au niveau des sources d'humidité en l'an 1840, les sources océaniques chaudes y produisant le plus d'humidité. (C) Le diagramme de la force de l'ENSO montre un changement de régime à la moitié du 19^{ième} siècle. Ce changement est lié à la contribution de la dépression des Aléoutiennes plus au sud.

Figure 4 compares $\delta(^{18}O)$ from the PRCol and Jellybean Lake core (Anderson, 2004; Anderson *et al*., 2004). The JBL record comes from carbonates and reflects the meteoric water values for the average catchment elevation of about 1 600 m asl. These two 2000-year-long series are very close indeed and both show the shift at A.D. 1840 and another similar shift about A.D. 800. There are other large changes in Figure 4 but we focus on these two because they are the main shifts in level.

Three questions spring to mind. First, what is behind the sudden shift at *ca*. A.D. 1840 and A.D. 800? Second, why does it have different strengths in δ expression depending on elevation (3.5, ~0.0 and 1.5 ‰ at PRCol, Eclipse and JBL respectively). Third, and most significant, why are the PRCol and JBL records "up-side-down" with the Little Ice Age having more positive δs when it is known from tree-ring studies that most of Alaska had a normally cold Little Ice Age.

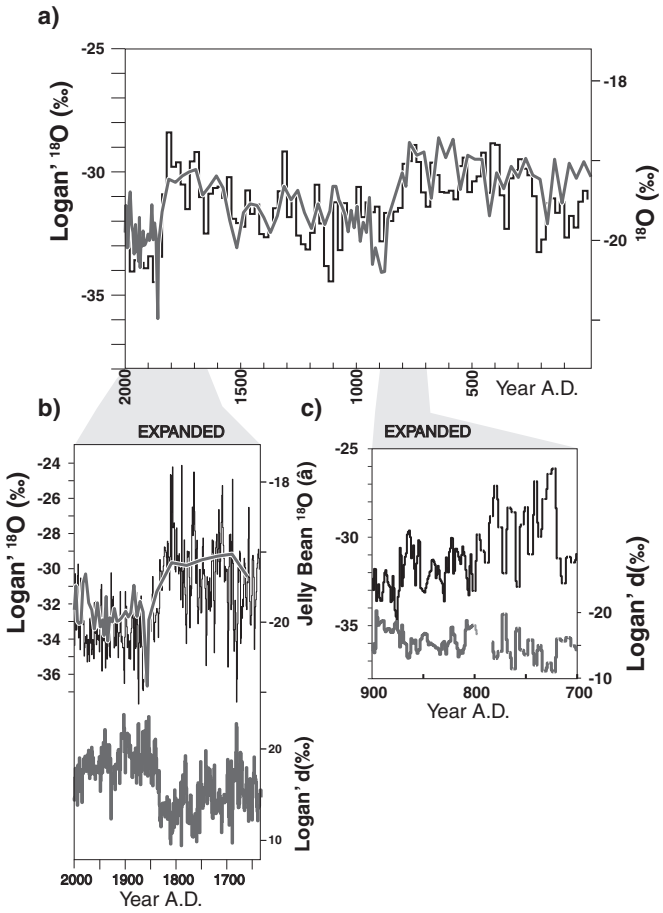

FIGURE 4. (A) The $\delta(^{18}O)$ records from Jellybean Lake and from PRCol with the sudden shifts in *ca*. A.D. 1840 and A.D. 800 appearing in both. There is a high degree of coherence between these records. The expanded inserts (B and C) show the highest resolution data from PRCol for $d(^{18}O)$ and annual deuterium excess (d) for the two sudden shifts. The $\delta(^{18}O)$ shift near A.D. 800 in C appears to have happened in less than 5 years and, like that in A.D. 1840, it is accompanied by a change in the level of the deuterium excess.

(A) Les séries temporelles de $\delta(^{18}O)$ du lac Jellybean et du forage de PRCol montrent des changements brusques en ca *A.D. 1840 et A.D. 800, une forte cohérence existant entre les séries temporelles. Les changements observés dans $\delta(^{18}O)$ et l'excès de deutérium annuel (d) du forage de PRCol sont illustrés à une haute résolution (en B et C). Le changement qui s'est produit en A.D. 800 dans la série $\delta(^{18}O)$ s'est effectué en moins de cinq années et, comme en A.D. 1840, il est accompagné d'un changement dans l'excès de deutérium.*

Previous work on the 300-years NWCol core (Holdsworth *et al*., 1992; Moore *et al*., 2002; Rupper *et al*., 2004) has shown that over recent times higher accumulation, which correlates in general with lower $\delta(^{18}O)$, comes in years that the Aleutian Low is deeper and the vapour flow lines originate farthest south. Having "more southern moisture sources" is another way of saying that meridional vapour flow is enhanced in high accumulation years at the 5 340 m level.

Mann *et al*. (2000) point out that the statistics of ENSO (Trenberth and Hoar, 1997) undergo an important shift in the middle 19th century (Fig. 3C). They conclude that a change occurred in the mid-1800s toward fewer long warm ENSO events. From a study of tropical records, Rein *et al*. (2004) conclude that there was a major weakening in El Ninõ in A.D. 800. Moore *et al*. (in press) have also concluded that a major shift in tropical teleconnection occurred at *ca*. A.D. 1850.

MODEL SIMULATIONS FOR THE MODERN REGIME

Two isotope simulations from the coast to the Mount Logan Plateau are presented. The first uses "modern" moisture sources (including tropical), and the second only North Pacific sources.

A semi-empirical model has been used in a wide range of polar situations, in simulating $\delta(^{18}O)$ and $\delta(D)$ (Fisher, 1990, 1991, 1992; Kavanaugh and Cuffey, 2003). For the modern situation, the model inputs multi-latitude sources and uses measured zonal annual averages of major water cycle variables such as evaporation rate, total meridional flux, precipitable water content, precipitation, sea temperature, wind speed, relative humidity, sea ice front, etc. Figure 5A-G shows the input fields used to model the present annual global water cycle isotopes and precipitation rates at sea level (adapted from Fig. 1 of Fisher, 1990). The survival distance for water vapour (shown in Fig. 5A) is the distance that a slug of source water travels north or south before losing 63 % (1/e) of its mass by precipitation. The survival time at a given point in the water cycle is measured by the total water content divided by the precipitation rate. The survival distance is obtained by multiplying this time by the average drift velocity of the water vapour (total vapour flux/total water content). All these quantities are known and the sources of data are referenced in the captions to Figure 5. This model successfully simulates the zonal annual average sea level $\delta(^{18}O)$ and d (Fig. 6A-B) as well as the precipitation rate. Figure 6C shows the simulated and measured values (Fisher, 1990, 1992).

The global model provides the initial values for a regional model that assumes moisture flux over land has a known trajectory (assumed to be perpendicular to precipitation rate isopleths) from the coast to a given site. The regional model is also empirically driven and requires precipitation, elevation and air temperature along the trajectory from the coast to the inland sites. A key element of the regional model is the weighting

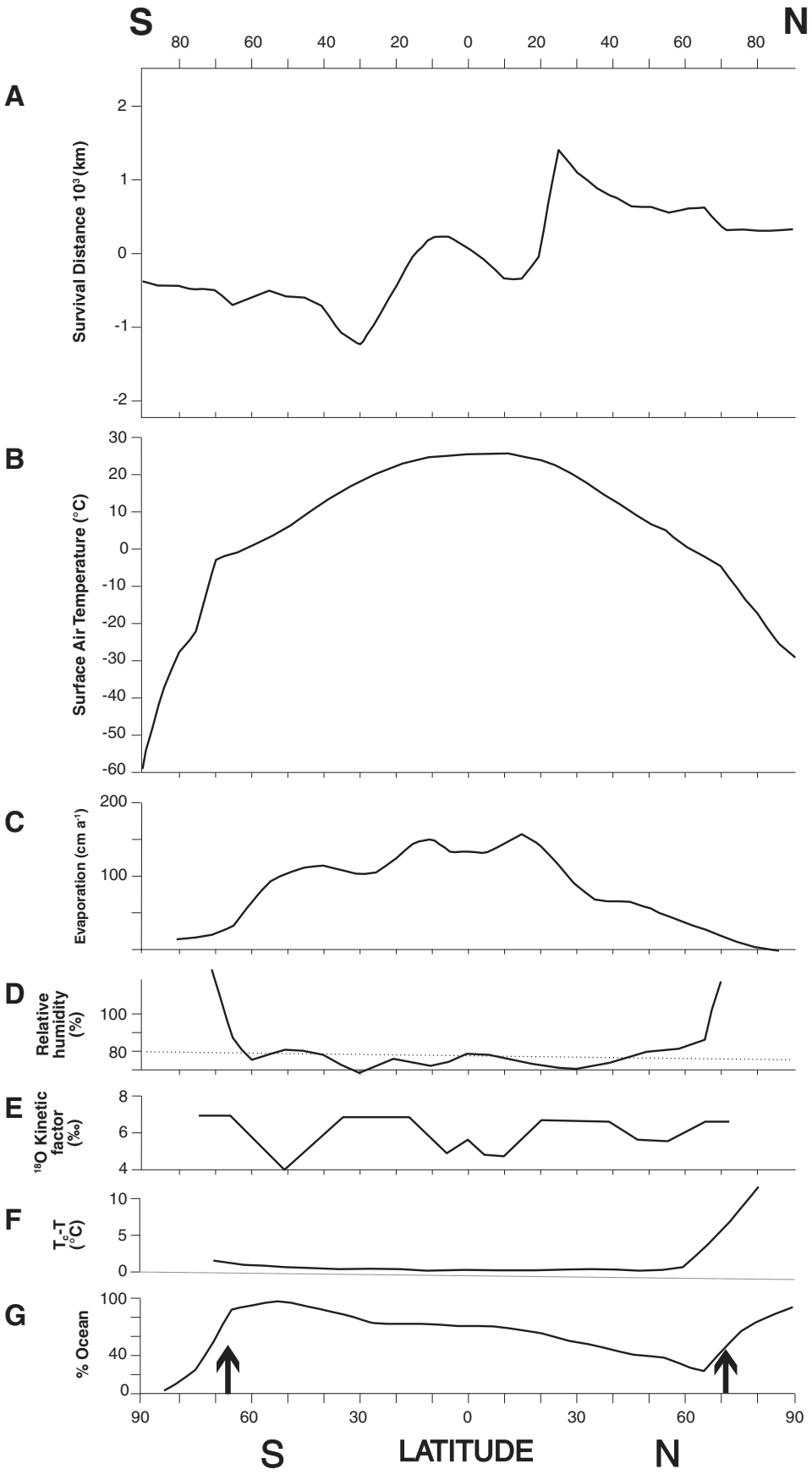

FIGURE 5. Modern annual zonal averages of annual input data fields for the isotope model, and model output compared to observations (Fisher, 1990). (A) Survival distance (km) for water vapour (l). Positive values indicate northward vapour transport. (B) Near-surface air temperature (T). (C) Evaporation rate (E). (D) Near-surface relative humidity (h). (E) Kinetic evaporation fractionation factor (k_{18}). (F) Difference between the sea temperature and the air temperature (T_c - T). (G) Percentage of the zone that is ocean with vertical arrows indicating the annual average position of the sea ice.

Moyennes annuelles des intrants et des extrants du modèle isotopique comparées aux observations (Fisher, 1990). (A) Distance de survie (km) de la vapeur d'eau (l). Les valeurs positives indiquent un transport vers le nord. (B) Température de l'air près de la surface (T). (C) Taux d'évaporation (E). (D) Humidité relative près de la surface (h). (E) Facteur de fractionnement d'évaporation cinétique (k_{18}). (F) Différence entre la température de la mer et la température de l'air (T_c - T). (G) Pourcentage de la zone dans l'océan (C), les flèches verticales indiquant la position relative des glaces de la mer.

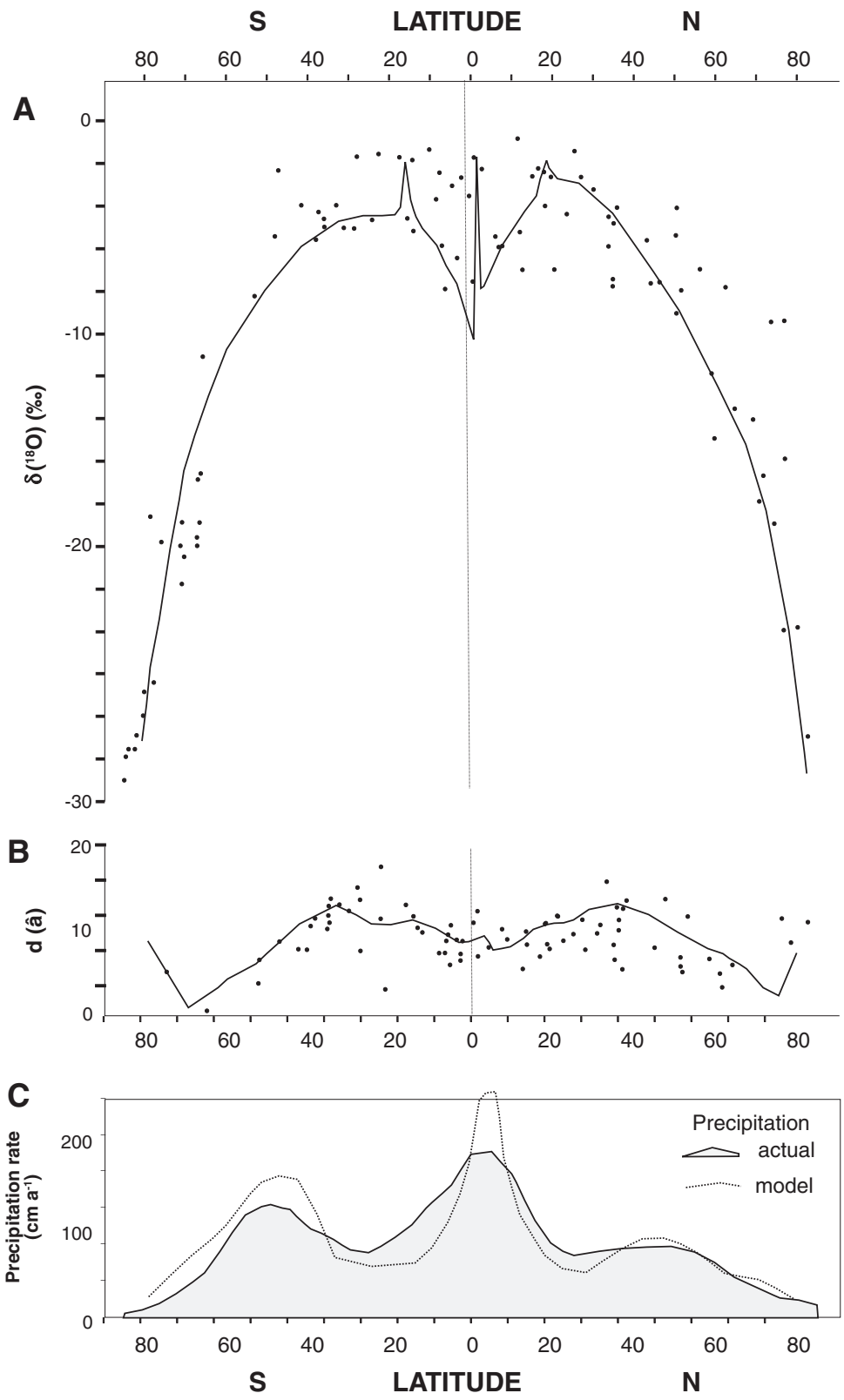

FIGURE 6. (A) Annual averages of $\delta(^{18}O)$ versus latitude. The dots are measured values and the line comes from the global model. (B) Annual deuterium excess, d, with dots from the measured data and the line from the model. The global runs assume ice clouds form at -10 °C, and the supersaturation in these clouds is after Jouzel *et al.* (1984) and Fisher (1990). (C) The measured annual zonal precipitation rates (shaded) and the model's calculations.

(A) Moyennes annuelles de $\delta(^{18}O)$ en fonction de la latitude. Les points sont les valeurs mesurées et la ligne est issue du modèle global. (B) Excès de deutérium annuel, d, où les points sont les valeurs mesurées et la ligne est issue du modèle global. La simulation présume que les nuages se forment à -10 °C et que leur supersaturation se fait d'après Jouzel et al. *(1984) et Fisher (1990). (C) Taux de précipitation annuels mesurés (ombragé) et calcul du modèle.*

given to moisture sources depending on the elevation of the site. Higher sites receive less local water. The weighting factor used in the model preserves the vertical profile for total precipitable water and simulates the need for a certain horizontal fetch L_x (= 2 500 km), to get moisture from a given ocean source up to elevation L_z (= 3 000 m asl) (Fisher, 1990). Examples of the regional model output for traverses up the Devon Island Ice Cap and up a line in East Antarctica are given in Figure 7 (Fisher, 1990). In both cases the accumulation rates and elevations are well known.

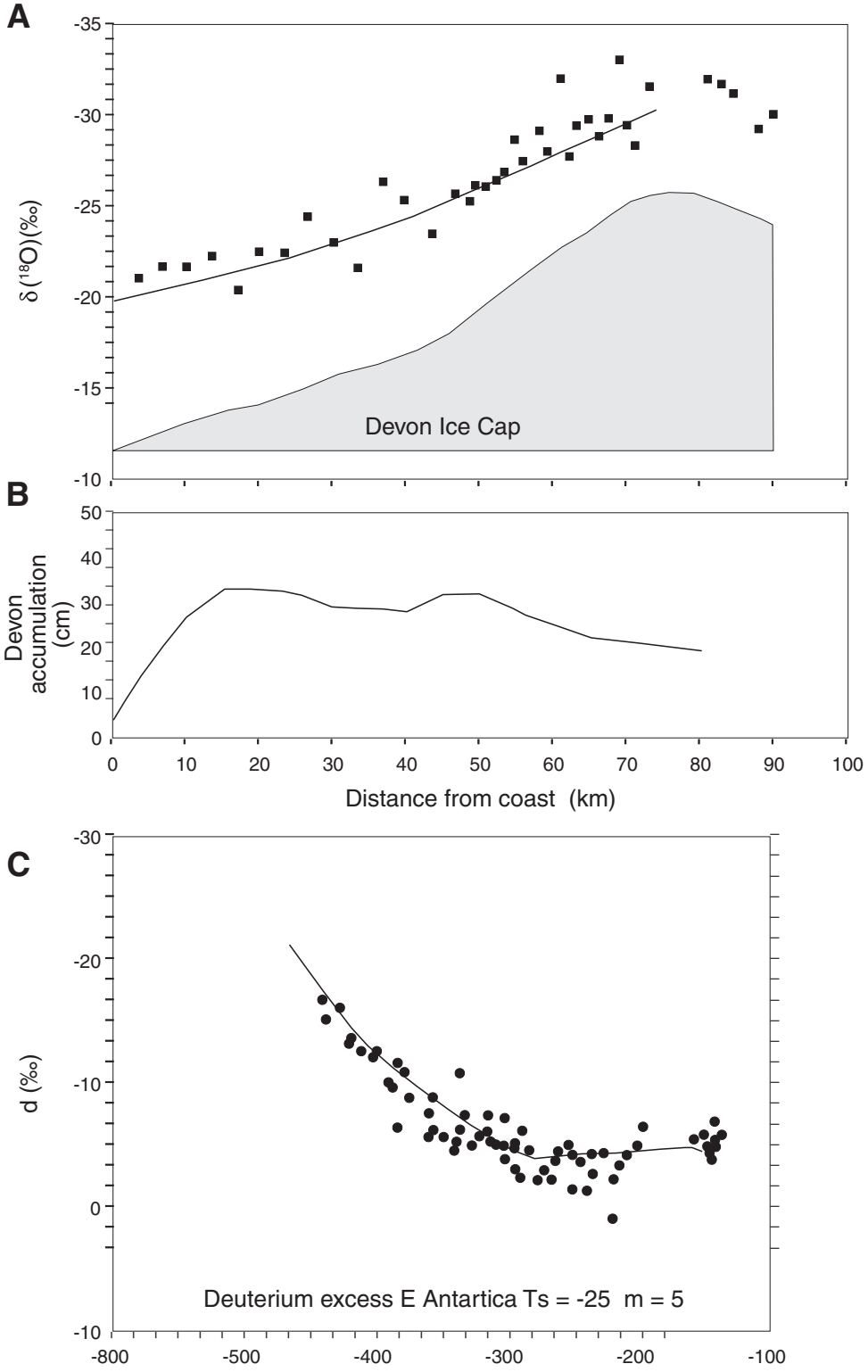

FIGURE 7. Example of the regional model for the southeast side of the Devon Ice Cap. (A) The $\delta(^{18}O)$ data (squares) and (B) the accumulation rate data (both from Koerner and Russell, 1979). The lines are predicted by the model (Fisher, 1992) using the measured accumulation and coastal values of $\delta(^{18}O)$. (C) An East Antarctic example of d versus $\delta(D)$ from observations (Petit *et al.*, 1991). The line is that predicted by the regional model (Fisher, 1992).

Exemple du modèle régional pour la partie sud-est de la calotte glaciare de Devon. (A) Données de $\delta(^{18}O)$ (carrés) et (B) taux d'accumulation (d'après Koerner and Russell, 1979). Les lignes sont prédites par le modèle (Fisher, 1992) à partir des accumulations mesurées et les valeurs côtières de $\delta(^{18}O)$. (C) Exemple de d en fonction de $\delta(^{18}O)$ à partir des observations (Petit et al., 1991) pour l'est de l'Antarctique. La ligne représente la prédiction du modèle régional (Fisher, 1992).

The accumulation rate data, average temperatures and moisture trajectories are not as well known in the St. Elias Mountains. However, substantial data from the "Icefield Ranges Research Project" along with new data gathered by us, may be used as an input set for the regional runs. Figure 8 (adapted from Marcus and Ragle, 1972) shows the accumulation rates and elevations from Yakutat to Kluane Lake. The expanded part (Fig. 8B) gives the data from Seward Glacier to the top of the Logan Plateau. The runs start at the coast (Yakutat) and end on the Logan Plateau. The annual average temperature at Yakutat, and our camps at Quinto Sella (QS), Eclipse (E), KingCol and PRCol are known. Linear interpolation with elevation is used in between. The Marcus and Ragle (1972) data have a blank between Yakutat and kilometre 60 in Figure 8A. The three numbered lines are each used as part of three input sets to the regional model, and the spread of results imposes uncertainty on the simulations. Another source of uncertainty in the input data is the value of the coastal precipitation rate, as the global model can only produce zonal averages of $\delta(^{18}O)$ and precipitation at the coast.

The modern predicted $\delta(^{18}O)$ and d from coastal Alaska to the top of Logan appear in Figures 9A and 9B as line-functions. The shaded areas show the range of simulations due to the geographic paucity and temporal spread in measured local accumulation rates. The points in Figure 9A represent measured $\delta(^{18}O)$ of surface samples taken over a wide range of years. Most of these points are from Holdsworth and Krouse (2002). This model captures most of the vertical $\delta(^{18}O)$ structure, including the recumbent section from about 3.0 to 4.8 km. Similarly Figure 9B presents the modeled and measured d for modern annual conditions. For each site (or elevation), the model output includes the relative importance of source ocean strips (*i.e.* the percentage of the accumulation that originates in each source ocean strip). For the modern regime (defined by Figs. 5 and 8), the source ocean contribution distributions for sites at 5 400, 2 900 and 1 300 m asl are plotted in Figure 10A. The PRCol site (5 400 m asl) normally receives relatively little local water, whereas the 1 300 m asl sites receive quite a lot.

MODEL EXPERIMENT FOR PURELY ZONAL SOURCES OF WATER

As an experiment to test the importance of water source, the model was fed only with water originating in the North Pacific strip defined by latitude range 40 °N to 60 °N and from the coast of Asia to North America (longitude 120 °E to 120 °W), with all southerly sources excluded. The empirical water cycle variables averaged in 15 longitude bins within this North Pacific rectangle are the input for the "pure zonal source" model run. Figure 11 shows the input data for this North Pacific source strip. In this experiment the survival distance (Fig. 11G) is found using only the zonal water vapour flux (Fig. 11E). This approach is taken to get the input "empirical data" *in lieu* of having the actual variables for a hypothetical pure zonal flow. As before, the model predicts the precipitation rate as a by-product. The dashed line in Figure 11C is the model precipitation rate and the step function is the measured rate. The size and first-order fit are good. The differences are due to the way the zonal regime has been constructed. Also the modeled precipitation requires mass conservation within its set of strips, clearly not met in this experiment. The overland portion of the model run assumes the same input accumulation and temperature fields as were used before in the St. Elias.

The main difference between the modern-ocean-source runs and this experimental North Pacific zonal-source is that the former includes tropical water with surface temperatures up to +30 °C and a weighted source mean of about +19 °C, whereas the latter experimental zonal run has ocean water strips all with temperatures about +10 °C. We hypothesize that, prior to A.D. 1840, North Pacific water fed the St. Elias via zonal flow, and that thereafter, modern flow has delivered water from all the possible southern latitudes. Because of the uncertainties in the hypothetical North Pacific input, a run is picked within these uncertainties to hit the pre-A.D. 1840 $\delta(^{18}O)$ average at PRCol. After this "fine tuning", the simulation for all the other elevations is objective. Figure 12A shows the simulated relation of [δ(zonal) - δ(modern)] versus elevation. The line is from the model runs and the squares are data from the three sites. The shading reflects the estimate of errors taken from Figure 9A. The PRCol difference is successfully modeled (as it must be), but what is pleasing is the success that the [model + hypothesis] has in forecasting the differences at the Eclipse and Jellybean Lake sites. Eclipse has virtually no shift and JBL has a 1.5‰ shift. The twin maxima at 1.3 and 5.4 km elevation in Figure 12A come about because of source weighting factors (Fig. 10). Switching the water source from warmer tropical to cooler northern oceans should affect the d substantially (Johnsen *et al.*, 1989), as is confirmed by the modeled difference of [d(zonal) - d(modern)] versus elevation (Fig. 12B). The difference is rather insensitive to elevation. The only value available for the d-difference is from PRCol, but the predicted shift is very close to the 4.5‰ shown in Figure 3C. This is a further validation of the hypothesis.

The level shift at A.D. 800 shown in the PRCol and JBL plots of Figure 4 is probably another regime shift. The PRCol Holocene record contains many such sudden and large shifts in $\delta(^{18}O)$ and d on the order of ~3 to 5 ‰.

This moisture source switch hypothesis can successfully reproduce abrupt changes in $\delta(^{18}O)$ at 5 400 and 1 300 m asl with no change at 3 000 m asl and changes in d at all elevations. However, other processes could also cause sudden changes. Scouring away of winter snow before A.D. 1840 could have produced similar changes (Fisher *et al.*, 1983), as could wind-enhanced vapour transport and isotopic fractionation (Neumann and Waddington, 2004). Both could be accomplished at the PRCol site by a sudden and systematic decrease in wind speeds at *ca.* A.D. 1840. This explanation would also apply to the older Logan core (Fig. 1C) that has a similar $\delta(^{18}O)$ shift, but it would fail to explain the change at Jellybean Lake or the zero shift at Eclipse. Given the amplitude of the seasonal $\delta(^{18}O)$ variation on the Logan Plateau, about 40 % of the year's accumulation (all the winter snow) would have to be removed to achieve a 3‰ shift in the annual average (Fisher *et al.*, 1993). There is no such large sudden change in the accumulation rate on the Plateau in the mid-1800s (Holdsworth *et al.*, 1992). In any case, hypothesizing such a sudden change in

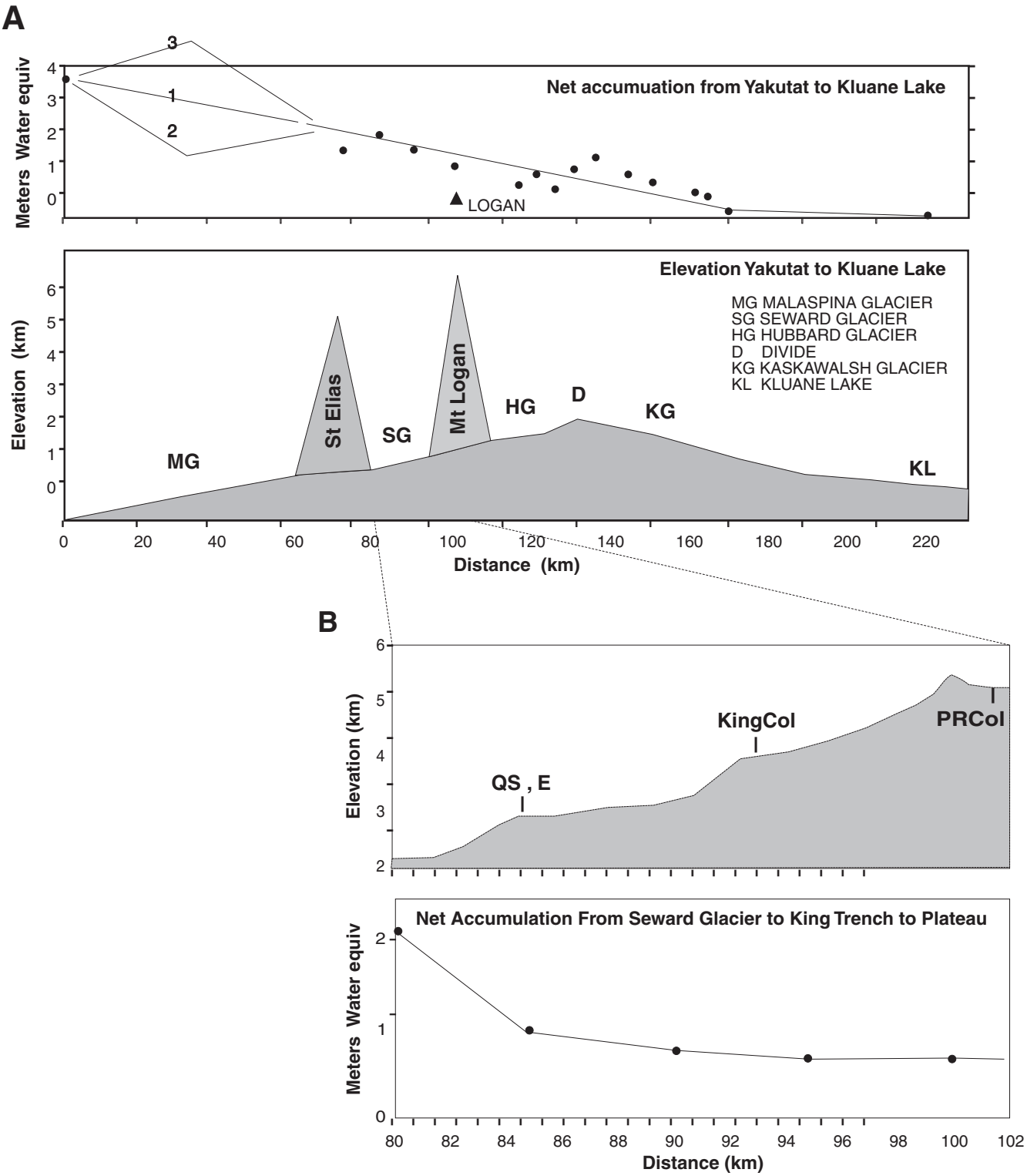

FIGURE 8. Regional input fields for "modern" St. Elias area. (A) Accumulation rates and elevations along a traverse from Yakutat on the Alaskan coast to Kluane Lake in the Yukon. (B) The expanded section from the upper Seward Glacier to the Mount Logan Plateau. The figure is adapted from Marcus and Ragle (1972) and supplemented with data collected by us in the Mt. Logan area. Ideally, model input of these variables should be along a traverse perpendicular to the accumulation isopleths. This ideal is not attainable, but the model results are close.

Intrants pour la région du mont St-Elias. (A) Taux d'accumulation et altitudes d'un transect entre Yakutat, sur la côte de l'Alaska, et le lac Kluane, au Yukon. (B) Agrandissement du transect entre le Haut Glacier de Seward et le Plateau du mont Logan. Cette figure est une adaptation de Marcus and Ragle (1972), combinée avec les données collectées par les auteurs dans la région du mont Logan. Idéalement, les intrants du modèle devraient être perpendiculaires aux lignes d'accumulation. Cet idéal est difficile à atteindre, mais les données utilisées dans le modèle s'en rapprochent.

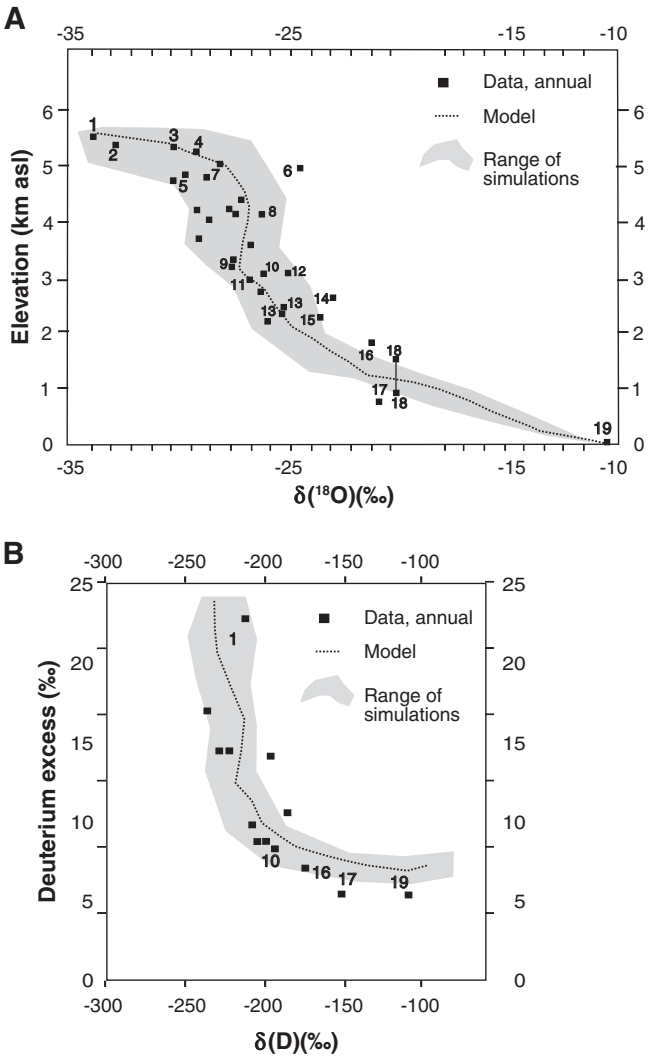

FIGURE 9. (A) Measured and modeled $\delta(^{18}O)$ for the St. Elias Mountains and South Yukon-Alaska. The shaded area shows the range of possible model results allowed by the uncertainties in the input data to the empirical model, and the line is the "best run". (B) Measured and modeled deuterium excess. The model used "modern" moisture delivery to the sites. The data points are from many researchers: (1) Logan Plateau (GH), (2) Prospector-Russell Col (GSC), (3) Logan Plateau PRNN (GH), (4) Windy Camp (GH), (5) Mount Churchill (GH), (6) Mount Bona (GH), (7) Football Field (GH), (8) King Col (GH, KA), (9) King Trench (GH, KA), (10) Eclipse (Kreutz, Yalcin, Wake), (11) Quintino Sella (GH, GSC), (12) (GH), (13) Rusty Glacier, (14) Divide (GH), (15) (GH), (16) Seward Glacier (GH), (17) Whitehorse, (18) Jellybean Lake, (19) Yakutat (GH). (GH = Gerrold Holdsworth; KA = Kumiko Azuma; GSC = Geological Survey of Canada).

(A) $\delta(^{18}O)$ mesuré et modélisé pour les montagnes St-Elias et le sud du Yukon-Alaska. La région ombragée montre les résultats possibles du modèle empirique liés aux incertitudes des intrants, et la ligne représente la meilleure simulation. (B) Excès de deutérium mesuré et modélisé, le modèle utilisant la production moderne d'humidité disponible aux sites. Les données proviennent de différents chercheurs: (1) Logan Plateau (GH), (2) Prospector-Russell Col (GSC), (3) Logan Plateau PRNN (GH), (4) Windy Camp (GH), (5) Mount Churchill (GH), (6) Mount Bona (GH), (7) Football Field (GH), (8) King Col (GH, KA), (9) King Trench (GH, KA), (10) Eclipse (Kreutz, Yalcin, Wake), (11) Quintino Sella (GH, GSC), (12) (GH), (13) Rusty Glacier, (14) Divide (GH), (15) (GH), (16) Seward Glacier (GH), (17) Whitehorse, (18) Jellybean Lake, (19) Yakutat (GH) (GH = Gerrold Holdsworth ; KA = Kumiko Azuma ; GSC = Geological Survey of Canada).

the wind is a large assumption, and it fails to explain the changes at the lower sites. Sudden and persistent changes in wind speeds might also be expected to be reflected in the chemical and dust loading in the ice cores. There is no such persistent change in the Eclipse core at A.D. 1840.

The moisture-switch hypothesis explains the relative changes at the three elevations, while the other processes do not. We will continue forward with this hypothesis. Holdsworth (2001) has examined the "statistical black box" of our simple model and attempted to model the vertical structure of the low pressure systems that deliver moisture storm by storm. His synoptic modeling will no doubt continue to throw more light on the detailed process changes that occur during one of the hypothesized regime changes.

DISCUSSION

The stable isotopes from the ice and lake cores from the southern Yukon paint a consistent picture of the Pacific water cycle over the last 2000 years and over a vertical range of nearly 5 000 metres. In this part of North America $\delta(^{18}O)$ is not a measure of past temperature but a "source-meter," indicating the relative connectedness of these Northern sites to either tropical or North Pacific water sources. There are sudden steps in $\delta(^{18}O)$ at PRCol and Jellybean Lake (*e.g.* A.D. 1840 and A.D. 800) which can be modeled by switching between modern-like and zonal water sources for these sites. What happens on Mount Logan and at JBL has some connection with the tropical winds. In the middle 1800s there is a shift in the statistics of ENSO (Fig. 3C; Mann *et al.*, 2000) from numerous long persistent warm-event ENSOs to fewer after A.D. 1850. Prior to A.D. 1840 we hypothesize mainly zonal source water for our suite of sites. This suggests that the North Pacific was more isolated from the south during the Little Ice Age, with a more southerly Polar Front (Mayewski *et al.*, 1994). The shift from zonal to modern vapor flux appears to have been abrupt and may have signaled the end of the Little Ice Age.

Thompson *et al.* (1986) and Hendy *et al.* (2002) have shown that pre-A.D. 1850, the trade winds in the Pacific were stronger than post-A.D. 1850 and (Moore *et al.*, in press) have related these stronger trade winds to a stronger Walker and weaker Hadley circulation pre-A.D. 1850. Similar conclusions are drawn from Antarctic ice cores (Mayewski *et al.*, 2004). The Eclipse accumulation rate is in anti-phase with that at the 5 400 m asl site, further demonstrating the vertical structure in water vapour transport (Yalcin *et al.*, 2004).

From a study of sea-ice-rafted debris from a core from the Emerald Basin off Nova Scotia, Keigwin *et al.* (2003) inferred that at about A.D. 1850 the export route of sea ice from the Arctic Ocean shifted from the west to the east side of Greenland. They hypothesize that a shift in the position of the "Icelandic Low" was responsible for this change. Meeker and Mayewski (2002) also attribute late Little Ice Age northern paleo-climate changes to shifts in the main pressure centres.

Another abrupt shift occurred in A.D. 800. Rein *et al.* (2004) find a very abrupt change in tropical and mid-latitude paleomoisture archives of both hemispheres in A.D. 800 and suggest that there were persistent weak El Ninõs between A.D. 800 and A.D. 1250 that were related to the Medieval

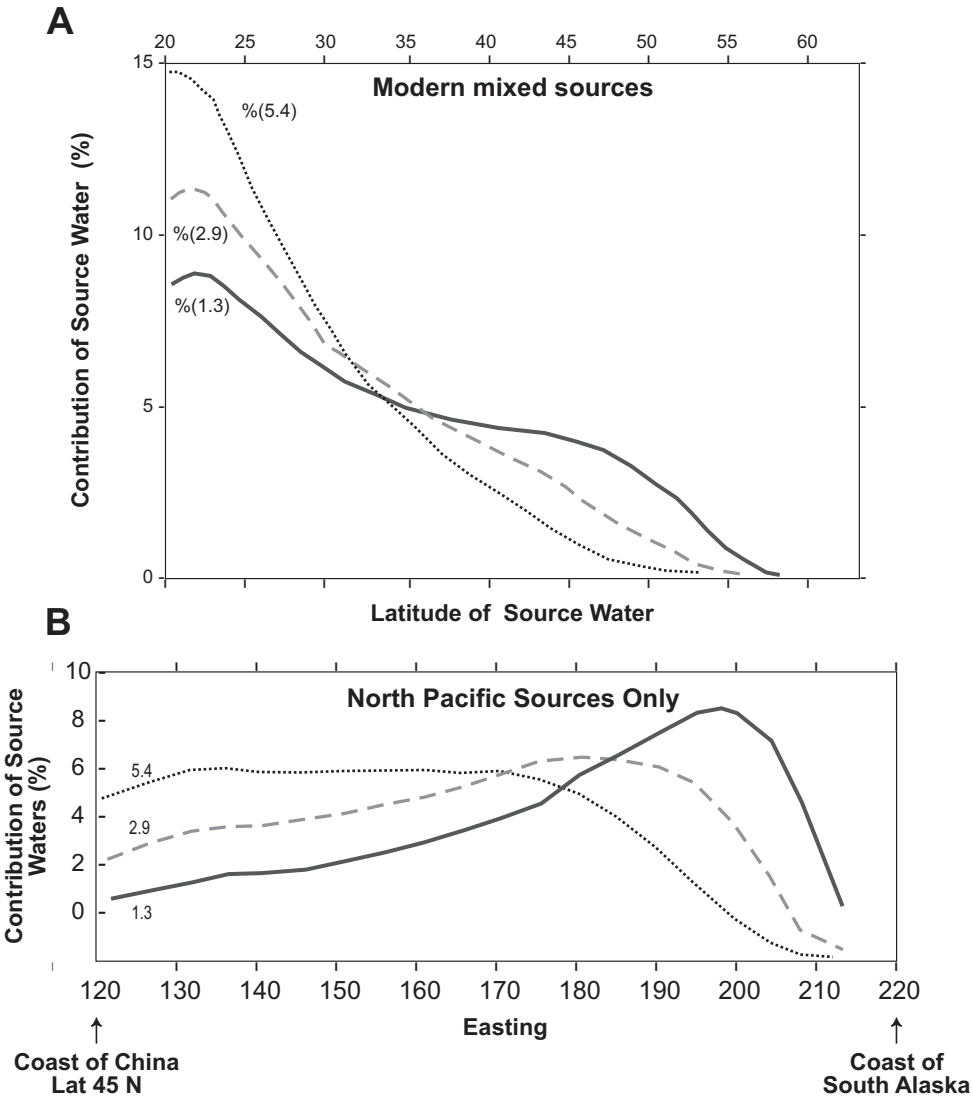

FIGURE 10. The moisture source contributions at three elevations in the St. Elias, assuming modern and "pure" North Pacific zonal regimes. It is these weighting functions that largely determine the modeled differences in stable isotope signatures at the various elevations. (A) Moisture source weightings for the modern regime and (B) for the purely North Pacific source strip experimental regime.

Les sources d'humidité à trois altitudes des monts St-Elias, le régime de la zone du Pacifique nord y étant considéré comme moderne et "pur". Ce sont les fonctions pondérées qui déterminent les différences observées dans les signatures isotopiques modélisées aux trois altitudes choisies. (A) Sources d'humidité pondérées pour le régime moderne et (B) le régime expérimental du Pacifique nord.

Warm Period. Their best-resolved series, a Peruvian drought index (from core 106KL), suggests the regime shift at A.D. 800 took less than a few decades. At PRCol, this shift occurred in less than 10 years (Fig. 4C). The period between A.D. 800 and A.D. 1250 was dry in Peru whilst core evidence from the Cariaco Basin core (ODP1002) suggests the Venezuelan side of South America was moist (Rein *et al.*, 2004).

The contention that the Northern Hemisphere wind-moisture flux system underwent a change in the middle of the 19th century seems to be consistent with many independent studies. The present work suggests that the changes in the mid-19th century leave their mark in the St. Elias-South Yukon $\delta(^{18}O)$ records because they are moisture source (not temperature) histories. The PRCol $\delta(^{18}O)$ history, having the best resolution, shows that these regime shifts happened quickly, within a year in the case of the A.D. 1840 shift. Preliminary analysis of the PRCol $\delta(^{18}O)$ Holocene record suggests that it contains many such shifts.

ACKNOWLEDGEMENTS

The field and laboratory work for these projects has been generously supported by International Arctic Research Center (IARC), the National Institute for Polar Research (Japan), the Geological Survey of Canada, the Niels Bohr Institute of the University of Copenhagen and the National Science Foundation (NSF grants OPP-0136005, OPP-0240878, OPP-0094587). The assistance of the Kluane Research Station manager Andy Williams (Arctic Institute of North America) was invaluable. The active help and cooperation of Gerrold Holdsworth is also gratefully acknowledged. The paper was improved through thorough reviews by Lloyd Keigwin, Steve Wolfe and an anonymous reviewer, and the editorial assistance of Barbara Stevenson.

REFERENCES

Anderson, L., 2004. Holocene climate from lake level and isotope analyses of small carbonate lakes, Yukon Territory, Canada. Unpublished Ph.D. thesis. University of Massachusetts at Amherst, 353 p.

Anderson, L., Abbott, M.B., Finney, B.P. and Burns, S.J., 2004. Regional atmospheric circulation change in the North Pacific during the Holocene inferred from Lascustrine carbonate oxygen isotopes, Yukon Territory, Canada. EOS, Transactions of the American Geophysical Union, 85, Fall meeting Supplement, Abstract PP23C-04.

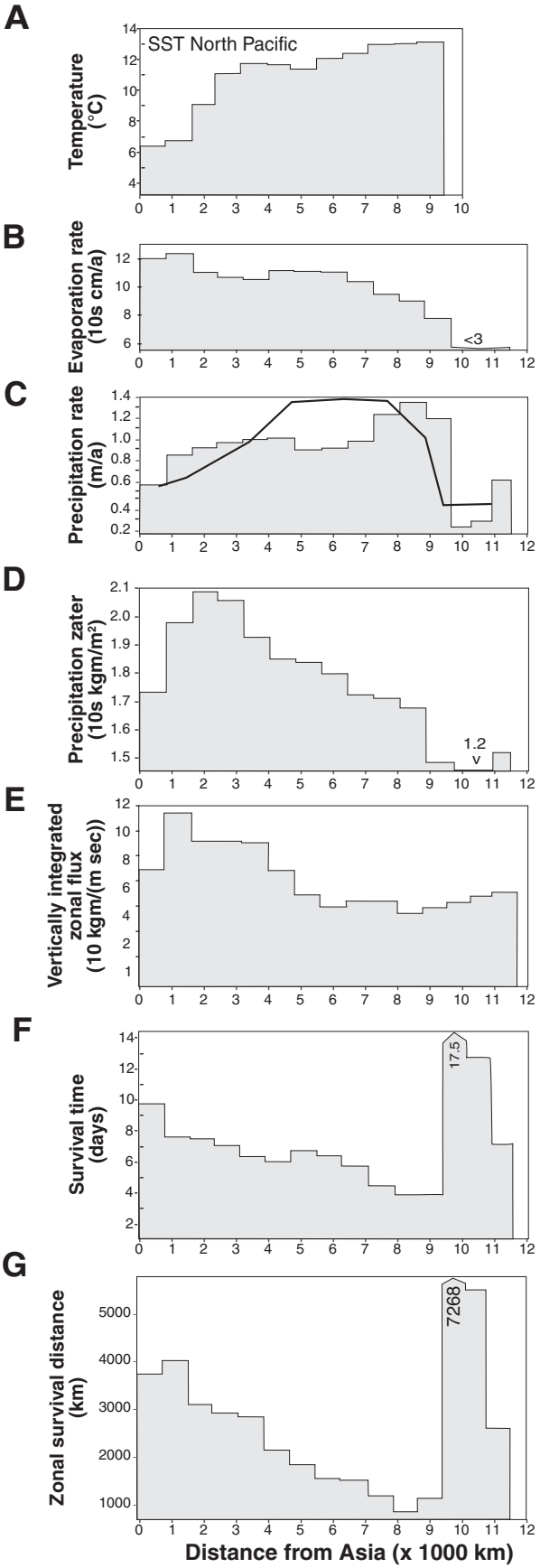

←

FIGURE 11. Empirical input data fields for the North Pacific Ocean strip from 40 °N to 60 °N and longitude range 120 °E to 120 °W. (A) Modern annual sea surface temperatures. (B) Evaporation rate annual averages (Peixóto and Oort, 1983). (C) Precipitation rate (Jaeger, 1983). The line is a model output, matching the input reasonably well given that mass conservation is not maintained in the numerical experiment that was carried out. (D) Total precipitable water in the atmosphere. (E) Measured annual average zonal water vapour flux (Peixóto and Oort, 1983). (F) Annual survival time (total precipitable water/precipitation rate), using Figures 10C and D. (g) Annual survival distance (zonal water vapour flux/precipitation rate) using Figures 10C and E. See Fisher (1990, 1992) for more details and explanations of the model input variables.

Données empiriques de l'Océan Pacifique nord entre 40 °N et 60 °N et entre 120 °E et 120 °W. (A) Températures annuelles modernes de la surface de la mer. (B) Taux d'évaporation annuels moyens (Peixóto and Oort, 1983). (C) Taux de précipitation (Jaeger, 1983). La ligne représente l'extrant du modèle et correspond très bien avec les intrants. (D) Total de l'eau précipitable dans l'atmosphère. (E) Flux de vapeur d'eau annuel moyen mesuré (Peixóto and Oort, 1983). (F) Temps de survie annuel (total de l'eau précipitable/taux de précipitation), estimé à partir des figures 10C et D. (G) Distance de survie annuelle (flux de vapeur d'eau/taux de précipitation), estimé à partir des figures 10C et E. Voir Fisher (1990, 1992) pour obtenir les détails et les explications sur les intrants du modèle.

Anderson, L., Abbott, M.B., Finney, B.P. and Burns, S.J., 2005. Regional atmospheric circulation change in the North Pacific during the Holocene inferred from Lascustrine carbonate oxygen isotopes, Yukon Territory, Canada. Quaternary Research, 64 : 21-35.

Clague, J.J., Evans, S.G., Rampton, V.N., and Woodsworth, G.J., 1995. Improved age estimates for the White River and Bridge River tephras, western Canada. Canadian Journal of Earth Sciences, 32 : 1172-1179.

Clausen, H.B., Hammer, C.U., Christensen, J., Schøtt-Hvidberg, C.S., Dahl-Jensen, D., Legrand, M. and Steffensen, J.P., 1995. 1250 years of global volcanism as revealed by central Greenland ice cores. NATO ASI Series I, 30, p. 517-552. *In* R.J. Delmas, ed., Ice Core Studies of Global Biogeochemical Cycles. Springer, New York, 402 p.

Cropper, J.P., 1982. Climate reconstructions (1801 to 1938) inferred from tree-ring width chronologies of the North American Arctic. Arctic and Alpine Research, 14 : 223-241.

Dansgaard, W., Johnsen, S.J., Clausen, H.B. and Gundestrup, N., 1973. Stable isotope glaciology. Meddeleser om Grønland, 197, 53 p.

Fisher, D.A., 1990. A zonally averaged stable-isotope model coupled to a regional variable-elevation stable isotope model. Annals of Glaciology, 14 : 65-71.

Fisher, D.A., 1991. Remarks on the deuterium excess in precipitation in cold regions. Tellus, 43B : 401-407.

Fisher, D.A., 1992. Stable isotope simulations using a regional isotope model coupled to a zonally averaged global model. Cold Regions Science and Technology, 21 : 61-77.

Fisher, D.A., 2002. High-resolution multiproxy climatic records from ice cores, tree rings, corals and documentary sources using eigenvector techniques and maps: assessment of recovered signal and errors. The Holocene, 12 : 401-418.

Fisher, D.A., Bourgeois, J.B., Demuth, M., Koerner, R.M., Parnandi, M., Sekerka, J., Zdanowicz, C., Zheng, J., Wake, C., Yalcin, K., Mayewski, P., Kreutz, C., Osterberg, E., Dahl-Jensen, D., Goto-Azuma, K., Holdsworth, G., Steig, E., Rupper, S. and Wasckiewicz, M., 2004. Mount Logan ice cores: the water cycle of the North Pacific in the Holocene. EOS, Transactions of the American Geophysical Union, 85, Fall Meeting Supplement, Abstract PP23C-07.

Fisher, D.A., Koerner, R.M., Kuivinen, K., Clausen, H.B., Johnsen, S.J., Steffensen, J.P., Gundestrup, N. and Hammer, C.U., 1996. Intercomparison of ice core $\delta(^{18}O)$ and precipitation records from sites in Canada and Greenland over the last 3500 years and over the last few centuries in detail using EOF techniques, p. 297-328. *In* P.D. Jones, R.S. Bradley and J. Jouzel, eds., Climate Variations and Forcing Mechanisms of the Past 2000 Years. Springer Verlag, Berlin, 649 p.

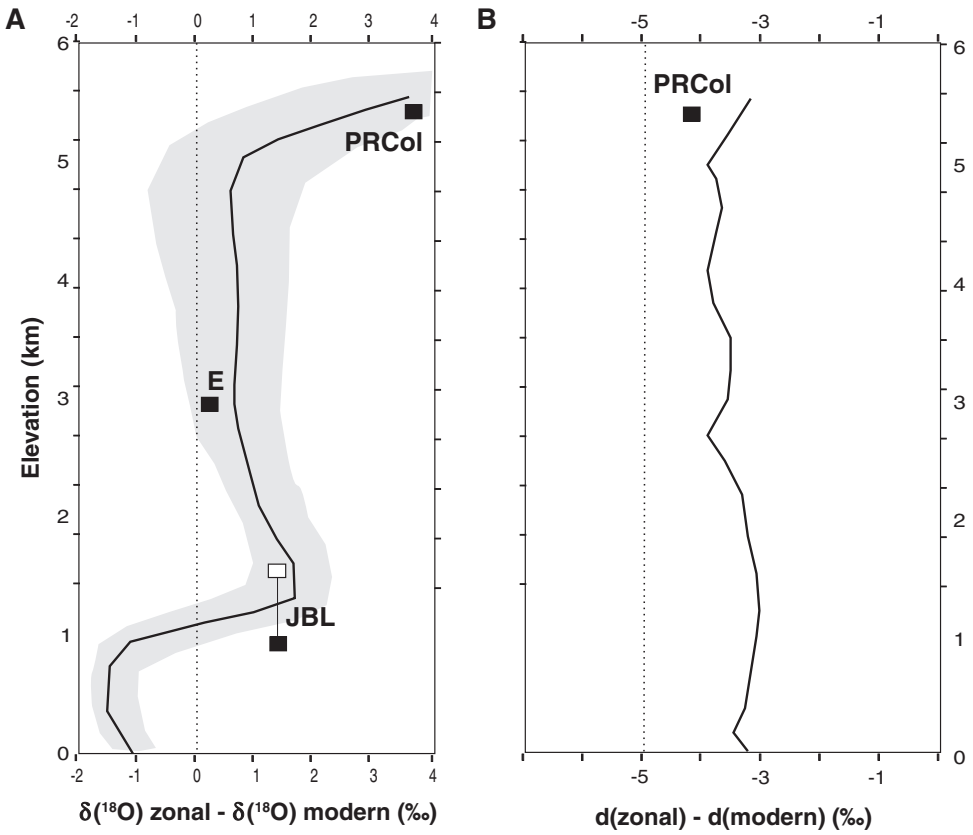

FIGURE 12. Predicted effects on (A) $\delta(^{18}O)$ and (B) d of shifting from a zonal (only North Pacific) moisture source to modern moisture sources (including tropical). The squares are the differences between pre- and post-A.D. 1840 $\delta(^{18}O)$ and d values in Figures 3 and 4 for the PRCol, Eclipse and Jellybean Lake sites. The shading around the [δ(zonal) - δ(modern)] versus elevation profile indicates the estimated errors taken over from Figure 5 and are mostly due to the lack of model-input accumulation data now and in the past. The elevation of Jellybean Lake is 800 m asl, but because it is in a valley surrounded by nearby mountains that provide runoff, the effective elevation is 1 650 m asl.

Effets prédits sur (A) $\delta(^{18}O)$ et (B) d du changement d'une source d'humidité zonale (Pacifique nord seulement) à des sources d'humidité modernes (incluant les tropicales). Les carrés représentent les différences entre $\delta(^{18}O)$ pré- et post-A.D. 1840 et les valeurs de d dans les figures 3 et 4 pour les sites PRCol, Eclipse et lac Jellybean. L'ombragé autour de [δ(zonal) - δ(moderne)] en fonction du profil d'élévation indique que les erreurs d'estimation issues de la figure 5 sont principalement dues au manque de données actuelles et passées dans le modèle. L'élévation du lac Jellybean est de 800 m asl, mais puisqu'il est situé dans une vallée entourée de montagnes qui contribuent au ruissellement, l'altitude effective est de 1 650 m asl.

Fisher, D.A., Koerner, R.M., Paterson, W.S.B., Dansgaard, W., Gundestrup N. and Reeh, N., 1983. Effect of wind scour on climatic records from ice-core oxygen–isotope profiles. Nature, 301 : 205-209.

Goto-Azuma, K., Shiraiwa, T., Matoba, S., Segawa, T., Kanamori, S., Fujii, Y. and Yomasaki, T.Y., 2003. An overview of the Japanese glaciological studies on Mt. Logan, Yukon Territory, Canada, in 2002. Bulletin of Glaciological Research, 20 : 65-72.

Hammer, C.U., 1983. Initial direct current in the buildup of space charges and the acidity of ice cores. The Journal of Physical Chemistry, 87 : 4099-4103.

Hendy, E.J., Gagan, M.K., Alibert, C.A., McCulloch, M.T., Lough, J.M., and Isdale, P.J., 2002. Abrupt decrease in tropical Pacific sea surface salinity at the end of the Little Ice Age. Science, 295 : 1511-1514.

Holdsworth, G.H., 2001. Calibration changes in the isotopic thermometer for snow according to different climatic states. Geophysical Research Letters, 28 : 2625-2628.

Holdsworth, G.H. and Krouse, H.R., 2002. Altitudinal variation of the stable isotopes of snow in regions of high relief. Journal of Glaciology, 48 : 31-41.

Holdsworth, G.H., Krouse, H.R. and Nosal, M., 1992. Ice core climate signals from Mount Logan Yukon A.D. 1700-1987, p. 483-504. *In* R.S. Bradley and P.D. Jones, eds., Climate Since A.D. 1500, Routledge, London, 525 p.

Jaeger, L., 1983. Monthly and areal patterns of mean global precipitation, p. 129-140. *In* A. Street-Perrott, M. Beran and R. Ratcliffe, eds., Variations in The Global Water Budget, R. Reidel Publishing Co., 518 p.

Johnsen, S.J., Clausen, H.B., Dansgaard, W., Gundestrup, N.S., Hammer, C.U.H., Andersen, U., Andersen, K.K., Hvidberg, S., Dahl-Jensen, D., Steffensen, J.P., Shoji, H., Sveinbjörnsdóttir, A.E., White, J., Jouzel, J. and Fisher, D., 1997. The $\delta(^{18}O)$ record along the Greenland Ice Core Project deep ice and the problem of possible Eemian climatic instability. Greenland Summit Ice Cores. Journal of Geophysical Research, 102(C12) : 26397-26410.

Johnsen, S.J., Dansgaard, W. and White, J.W.C., 1989. The origin of Arctic precipitation under present and glacial conditions. Tellus, 41B : 452-468.

Jouzel, J., Alley, R.B., Cuffey, K.M., Dansgaard, W., Grootes, P., Hoffmann, G., Johnsen, S.J., Koster, R.D., Peel, D., Shuman, C.A., Stievenard, M. and White, J., 1997. Validity of the temperature reconstruction from water isotopes in ice cores. Journal of Geophysical Research, 102(C12) : 26471-26488.

Jouzel, J., Merlivat, L. and Lorious, C., 1984. Deuterium and Oxygen 18 in precipitation: modeling of the isotopic effects during snow formation. Journal of Geophysical Research, 89(D7) : 11749-11757.

Kavanaugh, J.L. and Cuffey, K.M., 2003. Space and time variations of $d(^{18}O)$ and d(D) in Antarctic precipitation revisited, Global Biogeochemical Cycles, 17, 1017, doi: 10.1019/2002GB001910, 2003.

Keigwin, L.D., Sachs, J.P. and Rosenthal, Y., 2003. A 1600-year history of the Labrador Current of Nova Scotia. Climate Dynamics, 21 : 53-62.

Koerner, R.M. and Russell, R.D., 1979. $\delta(^{18}O)$ variations in snow on the Devon Island Ice Cap, Northwest Territories, Canada. Canadian Journal of Earth Sciences, 16 : 1419-1427.

Mann, M.E., Bradley, R.S. and Hughes, M.K., 2000. Long-term variability in El Niño-Southern Oscillation and associated teleconnections, p. 357-412. *In* H.F. Diaz and V. Markgraf, eds., El Niño and the Southern Oscillation, Cambridge University Press, 496 p.

Marcus, M.G. and Ragle, R.H., 1972. Snow accumulation in the Icefield Ranges, St. Elias Mountains, p. 130-142. *In* V.C. Bushnell and R.H. Ragle, eds., Icefield Ranges Research Project Scientific Results, Vol. 3. American Geographical Society, New York and Arctic Institute of North America, Montréal, 261 p.

Mashiotta, T.A., Thompson, L.G. and Davis, M.E., 2004. The White River ash: new evidence from the Bona-Churchill ice core record. EOS, Transactions of the American Geophysical Union, 85, Fall Meeting Supplement, Abstract PP21A-1369.

Mayewski, P.A. *et al.*, 1994. Changes in atmospheric circulation and ocean ice cover over the North Atlantic during the last 41 000 years. Science, 263 : 1747-1751.

Mayewski, P.A., Holdsworth, G., Spencer, M.J., Whitlow, S., Twickler, M., Morrison, M.C., Ferland, K.K. and Meeker, L.D., 1993. Ice core sulfate from three Northern Hemisphere sites: Source and temperature forcing implications. Atmospheric Environment, Part A, 27 : 2915-2919.

Mayewski, P.A., Maasch, K.A., White, J.W.C., Steig, E.J., Meyerson, E., Goodwin, I., Morgan, V.I., van Ommen, T., Curran, M.A.J., Souney, J. and Kreutz, K., 2004. A 700-year record of Southern Hemisphere extratropical climate variability. Annals of Glaciology, 39 : 127-132.

Mayewski, P.A., Meeker, L.D., Twickler, M.S., Whitlow, S., Yang, Q., Lyons, W.B. and Prentice, M., 1997. Major features and forcing of high-latitude northern hemisphere atmospheric circulation using a 110 000-year-long glaciochemical series. Journal of Geophysical Research, 102(C12) : 26345-26366.

Meeker, L.D. and Mayewski, P.A., 2002. A 1400-year high-resolution record of atmospheric circulation over the North Atlantic and Asia. The Holocene, 12 : 257-266.

Merlivat, L. and Jouzel, J., 1979. Global climatic interpretation of the deuterium-oxygen 18 relationship for precipitation. Journal of Geophysical Research, 84(C8) : 5029-5033.

Moore, G.W.K., Alverson, K. and Holdsworth, G., In press. Mount Logan ice core evidence for changes in the Hadley and Walker circulations following the end of the Little Ice Age. *In* R. Bradley and H.F. Diaz, eds., The Hadley Circulation: Past, Present and Future.

Moore, G.W.K., Holdsworth, G. and Alverson, K., 2001. Extra-tropical response to ENSO as expressed in an ice core from the Saint Elias Mountain range. Geophysical Research Letters, 28 : 3457-3460.

Moore, G.W.K., Holdsworth, G. and Alverson, K., 2002. Climate change in the North Pacific region over the past three centuries. Nature, 429 : 401-403.

Neumann, T.A. and Waddington, E.D., 2004. Effects of firn ventilation on isotopic exchange. Journal of Glaciology, 50 : 183-194.

Peixóto, J.P. and Oort, A.H., 1983. The atmospheric branch of the hydrological cycle and climate, p. 5-66. *In* A. Street-Perrott, M. Beran and R. Ratcliffe, eds., Variations in The Global Water Budget, R. Reidel Publishing Co., 518 p.

Petit, J.R., White, J.W.C., Young, N.W., Jouzel, J. and Korotkevich, Y.S., 1991. Deuterium excess in recent Antarctic snow. Journal of Geophysical Research, 96(D3) : 5113-5122.

Rein, B., Lückge, A. and Sirocka, F., 2004. A major Holocene ENSO anomaly during the Medieval period. Geophysical Research Letters, 31 : L17211.

Rupper, S., Steig, E.J. and Roe, G., 2004. The relationship between snow accumulation at Mt. Logan, Yukon and climate variability in the North Pacific. Journal of Climate, 17 : 4724-4739.

Thompson, L.G., Mosley-Thompson, E., Dansgaard, W. and Grootes, P.M., 1986. The Little Ice Age as recorded in the stratigraphy of the tropical Quelccaya Ice Cap. Science, 234 : 361-364.

Thompson, L.G., Mosley-Thompson, E.S., Zagorodnov, V., Davis, M.E., Mashiotta, T.A. and Lin, P., 2004. 1500 years of annual climate and environmental variability as recorded in Bona-Churchill (Alaska) ice cores. EOS, Transactions of the American Geophysical Union, 85, Fall Meeting Supplement, Abstract PP23C-05.

Trenberth, K.E. and Hoar, T.J., 1997. El Niño and climate change. Geophysical Research Letters, 24 : 3057-3060.

Wake, C.P., Yalcin, K. and Gundestrup, N.S., 2003. The climate signal recorded in the oxygen isotope accumulation and major-ion time series from the Eclipse ice core, Yukon Territory, Canada. Annals of Glaciology, 35 : 416-422.

West, K.E. and Krouse, H.R., 1972. Abundances of Isotopic Species of water in the St. Elias Mountains, p. 117-130. *In* V.C. Bushnell and R.H. Ragle, eds., Icefield Ranges Research Project Scientific Results, Vol. 3. American Geographical Society, New York and Arctic Institute of North America, Montréal, 261 p.

Whitlow, S., Mayewski, P.A. and Dibb, J.E., 1992. A comparison of major chemical species seasonal concentration and accumulation at the South Pole and Summit, Greenland. Atmospheric Environment, 26A : 2045-2054.

Wolfe, E., Moore, J.C., Clausen, H.B. and Hammer, C.U., 1997. Climate implications of background acidity and other chemistry derived from electrical studies of the Greenland Ice Core Project ice core. Journal of Geophysical Research, 102(C12) : 26325-26332.

Yalcin, K. and Wake, C.P., 2001. Anthropogenic signals recorded in an ice core from Eclipse Icefield, Yukon Territory, Canada. Geophysical Research Letters, 28 : 4487-4490.

Yalcin, K. and Wake, C.P., 2003. A 100-year record of North Pacific volcanism in an ice core from Eclipse Icefield, Yukon Territory, Canada. Journal of Geophysical Research, 108(D1) : 4012.

Yalcin, K., Wake, C.P., Whitlow, S.I., and Kreutz, K.J., 2004. Forest fire signals recorded in ice cores from Eclipse Icefield, Yukon Territory, Canada. EOS, Transactions of the American Geophysical Union, 85, Fall Meeting Supplement, Abstract PP23C-06.

Zheng, J., Kudo, A., Fisher, D.A., Blake, E.W. and Gerasimoff, M., 1998. Solid electrical conductivity (ECM) from four Agassiz ice cores, Ellesmere Island, NWT, Canada: High-resolution signal and noise over the last millenium and low resolution over the Holocene. The Holocene, 8 : 413-421.